Synthetic Metals 210 (2015) 352–356

Contents lists available at ScienceDirect

Synthetic Metals

journal homepage: www.elsevier.com/locate/synmet

Analysis of the ac response of an organic bulk-heterojunction solar cell based on AnE-PVstat:PCBM

M. Radaoui[a,b,*], A.Ben Fredj[a], S. Romdhane[a,c], D.A.M. Egbe[b], N.S. Sariciftci[b], H. Bouchriha[a]

[a] Laboratoire Matériaux Avancés et Phénomènes Quantiques, Faculté des Sciences de Tunis, Université El Manar, 2092 Campus Universitaire, Tunis, Tunisia
[b] Linz Institute for Organic Solar Cells (LIOS), Johannes Kepler University Linz, Altenbergerstr. 69, 4040 Linz, Austria
[c] Faculté des Sciences de Bizerte, 7021 Zarzouna, Bizerte, Université de Carthage, Tunisia

ARTICLE INFO

Article history:
Received 22 June 2015
Received in revised form 3 August 2015
Accepted 30 October 2015
Available online 14 November 2015

Keywords:
Negative capacitance
Negative electrical contact resistance
Diffusion length

ABSTRACT

We report an analysis of the ac response of a bulk-heterojunction solar cell in a standard architecture made of an anthracene containing poly(p-arylene-ethynylene)-alt-poly(p-arylene-vinylene)/1-(3 methoxy carbonyl) propyl-1-phenyl[6,6] and C_{60} (AnE-PVstat:PCBM) blend, these were made in detail at room temperature. Impedance spectroscopy is showing "backwards" arcs in Cole–Cole figures at low frequencies that are interpreted through equivalent circuit using negative resistances for electrical contacts. This equivalent circuit model incorporated chemical capacitance (C_μ), recombination resistance (R_{rec}), transport resistance (R_t) and contact electrical resistance (R_{co}). We have taken R_{co} as negative values in the bipolar regime to theoretically reproduce the small arc shown in the Nyquist plots. In addition, negative capacitance (NC) was observed under positive dc biases in the bipolar regime. The recombination time τ_{rec}decreases with increasing bias voltages. This result is in agreement with the direct Langevin-type bimolecular recombination. We determined the diffusion time (τ_{dif}) and the diffusion length (L_n) and other parameters. Average mobility of global carriers for the device is around $4\,10^{-3}\,cm^2\,V^{-1}\,s^{-1}$ which is in good agreement with that derived using PCBM electron-only devices.

1. Introduction

Organic solar cells are an attractive worldwide research subject because they are cheap, thin, lightweight and flexible. These characteristics make the organic solar cells easy to implement and usable for a variety of purposes [1–3]. One of the most promising solar cells that are having a rapid progression of improvements [4,5] are made from conjugated polymers and fullerenes in which a large heterointerface is achieved using the so-called bulk-heterojunction (BHJ) morphologies. Generally, both organic components are mixed in a common solvent, and after the deposition of this solution and subsequent annealing treatments, an optimal structure may be achieved with an average domain size on the order of the exciton diffusion length. The BHJ structure consists of percolated domains of an electron donor (conjugated polymers) and electron acceptor (fullerene or derivatives). This characteristic domain facilitates the exciton dissociation, maximizes the carrier generation efficiency [6], and achieves power conversion efficiency near 10% [7]. In order to design new materials for higher efficient devices, deep understanding of charge carriers diffusion processes in general is needed. Admittance spectroscopy has proved to be a powerful and a non-destructive method to study the internal electrical processes occurring in organic photovoltaics (OPVs) devices. The transport properties and the frequency dependent behavior yield give useful information about the physicochemical properties of a wide variety of electronic devices [8–9]. Impedance analysis has been applied to obtain the average charge carrier lifetime, the electronic density of states, and the charge carrier concentrations [10,11].

This work emphasizes the low frequency (ω) regime (under 1 MHz) where a negative contribution to the capacitance has been observed in some devices [12–14]. Different explanations for this negative capacitance (NC) have been presented including the minority carrier flow [15], the interface states [16], the slow transient time of injected carriers [17], the charge trapping [18] or the space charge [19]. In components exhibiting NC, the reactance is positive at low frequencies, and the resistance initially increases with frequency. When present, this trend is apparent in the cole–cole impedance plot as a region which extends into the fourth quadrant and exhibits the aforementioned increase in resistance as a function of frequency [20]. In literature, different equivalent circuit models have been proposed to simulate the impedance of

* Corresponding author.
E-mail address: raddaouimoufid@gmail.com (M. Radaoui).

http://dx.doi.org/10.1016/j.synthmet.2015.10.028
0379-6779/

organic solar cells (OSCs): (i) the simple parallel RC model, which results in perfect semicircular cole–cole diagrams, (ii) the parallel R-CPE model used in [21], that results in depressed circular diagrams. This circuit includes an extra fitting parameter to model non ideal non-homogeneities such as porosities, roughness and surface states (iii) The Mani parallel model [22], which consists in a parallel R_1CPE_1 in parallel with a series combination of R_2 and a second constant phase element CPE_2, (iv) Belmonte transmission line model, which includes distributed transport resistors, R_t, standing for carrier transport, and a distributed chemical capacitance C_μ, in parallel with a recombination resistance R_{rec} [23].

The active layer in the used device consists of an anthracene containing poly(p-phenylene-ethynylene)- alt-poly(p-phenylene-vinylene) (PPE-PPV) denoted AnE-PVstat [24], exhibits a very good ambipolar behavior consistent with reversible electrochemical oxidation and reduction peaks as well as a very good delocalization of HOMO (Highest Occupied Molecular Orbital) and LUMO (Lowest Unoccupied Molecular Orbital) levels [24]. AnE-PVstat is one of the most promising ambipolar materials for its high performance in OLEDs [25,26] and OPVs [24] devices.

In this letter, we probe the charge transport properties of bulk heterojunction (BHJ) blend by admittance spectroscopy. Under bipolar regime condition, the cole–cole impedance plots, in which clearly arcs toward the origin with two semicircles, and possesses positive reactance values. The observed cole–cole plots are modeled using the transmission line model, and from the fits to experimental data several parameters such as recombination resistance (R_{rec}), transport resistance (R_t), chemical capacitance (C_μ), the diffusion time (τ_{dif}), diffusion length (L_n) and many other parameters. The negative capacitance dominates at low frequencies. We associate this NC with slow electron hole bimolecular recombination at the heterojunction interface. Average mobility of global carriers for the device is around $4\,10^{-3}\,cm^2\,V^{-1}\,s^{-1}$ which is in good agreement with that derived using PCBM electron-only devices.

2. Experimental

The anthracene containing poly- (p-arylene ethynylene)-alt-poly(p-arylene-vinylene) s, abbreviated AnE-PVstat, was synthesized according to the procedures described previously [24,27]. The hole transport layer material, poly (3, 4-ethylene dioxythiophene) (PEDOT) doped with poly (styrene sulfonic acid) (PSS) (PEDOT:PSS Clevios P500), was purchased from Heraeus and *n*-type semiconductor phenyl C_{60} butyric acid methyl ester ($PC_{60}BM$) was from Sigma–Aldrich. PCBM were used in the structure of active layer without further purification. The AnE-PVstat and PCBM were firstly mixed in chlorobenzene with 1:2 (wt/wt) ratios. In solar cell fabrication process, ITO coated glasses were firstly subject to a standard cleaning process in an ultrasonic bath with de-ionized water, acetone, and isopropyl alcohol successively for 15 min and dried with dry nitrogen. The pre-cleaned ITO substrates were first treated with UV-ozone for 5 min. After that, the hole transport layer PEDOT: PSS was spin coated at 3000 rpm on the substrates and then annealed at140 °C on a hot plate for 10 min. Afterwards, fullerene -polymer blend was spin-coated at 1000–1200 rpm and immediately transferred inside nitrogen glove-box. The film of the fullerene–polymer blend was dried in vacuum (ca. 10^{-3} mbar) at ambient temperature for 30–40 min. Afterwards, top electrodes were deposited in vacuum $\sim 10^{-6}$ mbar. A combination of 1 nm of lithium fluoride (LiF) and 120 nm of Aluminum (Al) were used as the top electrode in the solar cell. The obtained device (thickness about 200 nm) was characterized directly inside the nitrogen glove box. Current–voltage characteristics of the sample were analyzed with Keithley 2400 source-measure and Solar Simulator under AM 1.5 G (80 mW/cm^2) standard characterization regulations. Solar Simulator was calibrated with a reference photodiode. An HP 4284A LCR-meter operated in the frequency range 20–10^6 Hz (v_{ac} = 20 mV ac voltage) was used to measure in the dark the complex admittance $Y(\omega)$, from which the capacitance $C(\omega) = ImY(\omega)/\omega$ and the conductance $G(\omega) = ReY(\omega)$ were extracted. We have carefully analyzed the low frequency regime in order to make sure that the extracted $C(\omega)$ and $G(\omega)$ are not influenced by any parasitic circuit reactance [28].

3. Results and discussions

Fig. 1 shows a semilog plot of the current versus applied voltage characteristic of ITO/PEDOT:PSS/AnE-PVstat:PCBM/LiF/Al structure, for both polarities under dark and illuminated conditions. As inferred from the plot, the structure possesses diode behavior in dark ambience. Under light exposure, the device shows the solar cell behavior. This solar cell exhibits a saturation current density J_{SC} = 6.5 mA/cm^2, an open circuit voltage V_{OC} = 0.8 V and fill factor FF = 60% resulting in a power conversion efficiency PCE = 3.6%. In the inset, we present the schematic structure of our solar cell.

Fig. 2a and b shows a cole–cole impedance plots of the ITO/PEDOT:PSS/AnE-PVstat:PCBM (1:2)/LiF/Al organic solar cell biased at 0 V, 0.5 V, 1 V and 1.5 V. Impedance spectroscopy is showing "backwards" arcs in cole–cole figure (Fig. 2b) at low frequencies. This is interpreted through equivalent circuits using negative resistances for electrical contacts.

The device structure is composed of three parts that can help us to modulate the cole–cole impedance plots. The interface between the transparent contact layer, which is indium tin oxide (ITO) and the active layer, could rise to a series resistance R_s which reflects passive resistors such as wires or ohmic contacts. The main cause that can affect R_s is the charge carrier transport within the active layer [29]. Like P3HT:PCBM, the investigation of charge transport properties in AnE-PVstat:PCBM device has revealed that carriers are collected into the electrodes through the competing mechanisms of diffusion-recombination [29], gives rise to equivalent circuits comprising distributed elements that are usually drawn in terms of transmission model given by Belmonte et al. [23].

Fig. 3 shows the equivalent circuit related to ITO/PEDOT:PSS/AnE-PVstat: PCBM/LiF/Al device studied in this work, comprising circuit distributed elements: transport resistance $r_t = R_t/L$(L is the active layer thickness) related to electron transport, recombination resistance $r_{rec} = R_{rec}/L$, chemical capacitance $C_\mu = C_\mu/L$, a

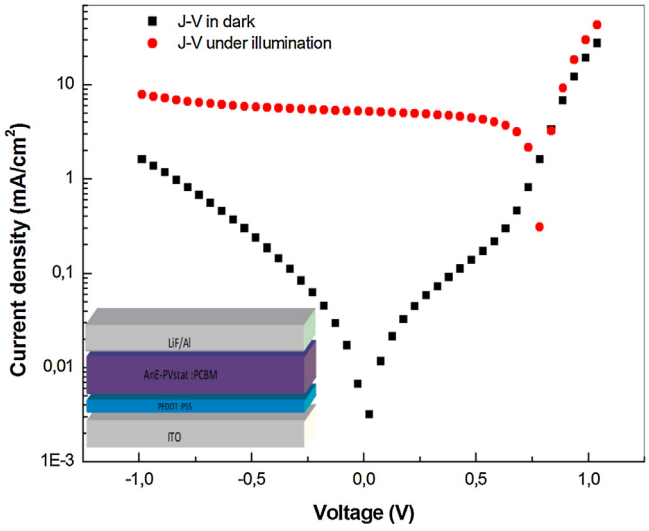

Fig. 1. J–V characteristic of the ITO/PEDOT:PSS/AnE-PVstat:PCBM/LiF/Al solar cell under simulated AM1.5G (80 mW/cm^2) irradiance.

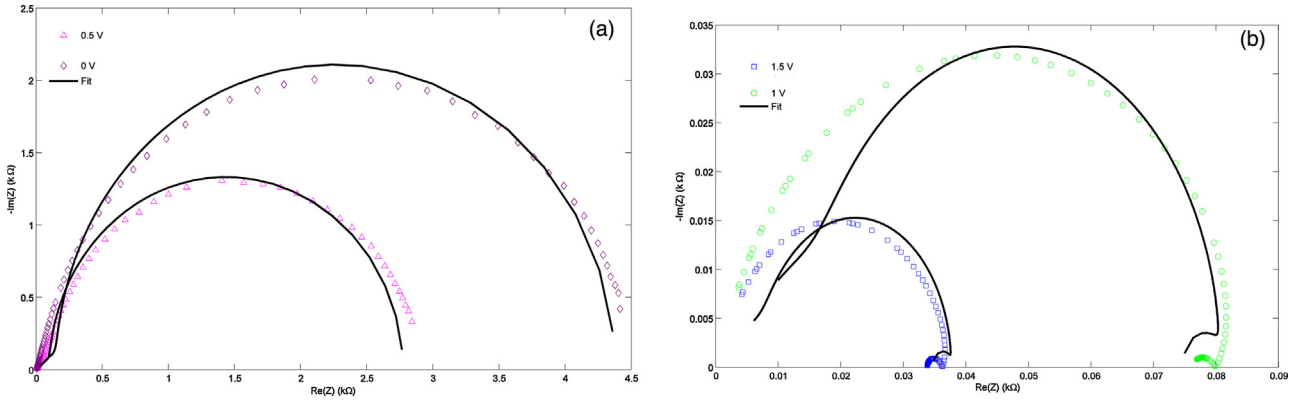

Fig. 2. Open symbols showing the cole–cole plots of ITO/PEDOT:PSS/AnE-PVstat:PCBM/LiF/Al based solar cell at various forward bias voltages: (a) Unipolar regime at 0 V and 0.5 V and (b) bipolar regime at 1 V and 1.5 V. Solid lines show the fit using the transmission line model proposed by Belmonte et al. [23].

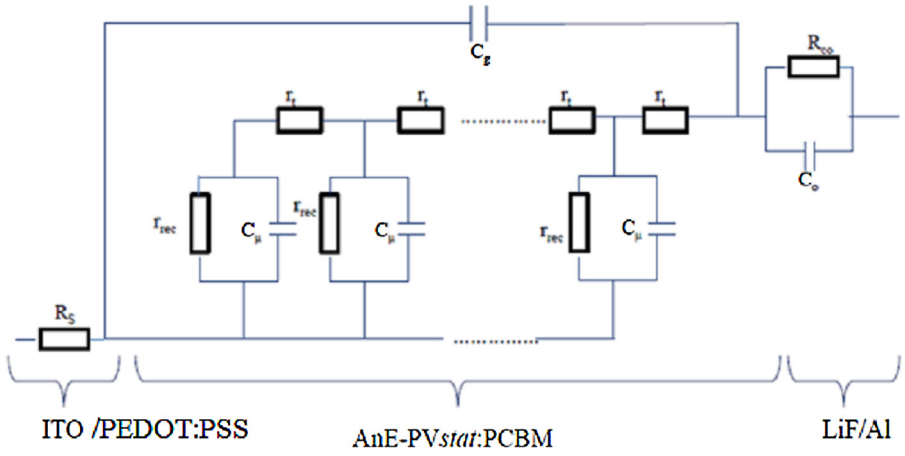

Fig. 3. Equivalent circuit related to ITO/PEDOT:PSS/AnE-PVstat:PCBM/LiF/Al based solar cell.

geometrical capacitance C_g and series resistance R_S that are connected to the last circuit (transmission line model). Contact electrical response is modeled by means of R_{co} in parallel with C_o.

The impedance (Z) can be solved analytically, and it is expressed by [29]:

$$Z = R_S + \sqrt{\left(\frac{R_t R_{rec}}{1 + i\frac{\omega}{\omega_{rec}}}\right)} \coth\left[\sqrt{\frac{\omega_{rec}}{\omega_d}}\sqrt{1 + i\frac{\omega}{\omega_{rec}}}\right] + \frac{R_{co}}{1 + i\omega R_{co} C_o} \quad (1)$$

Here, $\omega_d = 1/R_t \quad C_\mu = D_n/L^2$ (D_n being the electron diffusion coefficient) is the effective diffusion rate in a finite layer and $\omega_{rec} = 1/R_{rec}C_\mu$ is the recombination.

The fits of the experimental cole–cole impedance plots are given in Fig. 2. In this figure, we have shown a good agreement between experiments and theoretical results given by Eq. (1).

The impedance model described above contains two characteristic times related to electron diffusion (transit time), $\tau_{diff} = R_t C_\mu$ and the recombination time (effective lifetime), $\tau_{rec} = R_{rec} C_\mu$ respectively [23]. In addition, the diffusion constant, which describes the electron diffusivity (chemical diffusion coefficient), can be calculated through the relationship [23]: $D_n = L^2/\tau_{diff}$. With the latter expression, we can deduce the diffusion length, which is defined as an average distance in which mobile carriers can diffuse before recombination, and is related to the diffusion coefficient by $L_n = \sqrt{D_n \tau_{rec}}$. In addition, an estimation for the electron mobility is calculated using the Nernst–Einstein relationship as $\mu_n = qD_n/k_BT$ (k_BT is the thermal energy, where q is the elementary charge of electron, k_B is the Boltzman constant and T is the temperature) [29].

From the fits to experimental data, we have extracted the parameters cited above and that are summarized in Table 1 .

Fig. 4 shows the measured frequency dependent capacitance of the ITO/PEDOT:PSS/AnE-PVstat:PCBM (1:2)/LiF/Al device in the dark and at various applied forward bias voltages. For V > 0.5 V, we

Table 1
Summarized parameters extracted from the fits to experimental data of cole-cole impedance and capacitance plots shown on Figs. 2 and 4 respectively.

Voltages	Parameters										
	C_μ(nF)	C_{co}(μF)	R_{co}(Ω)	R_S(Ω)	R_t (Ω)	R_{rec} (Ω)	τ_{dif}(μs)	τ_{rec} (μs)	D_n (10^{-6} cm^2 s^{-1})	L_n(nm)	μ_n(cm^2 V^{-1} s^{-1})
0 V	15	10	4	2	4500	42230	67.5	633.5	5.9	–	–
0.5 V	20	20	2	2	3000	26700	60	534	6.6	–	–
1 V	30	40	−50	2	530	640	16	19.2	25	219	3.9 10^{-3}
1.5 V	40	80	−30	2	220	300	9	12	44	230	4 10^{-3}

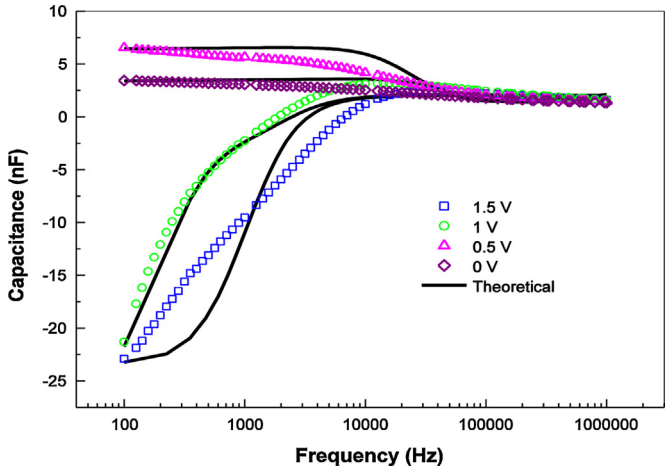

Fig. 4. Open symbols showing the measured capacitance versus frequency for ITO/PEDOT:PSS/AnE-PVstat:PCBM (1:2)/LiF/Al based solar cell at various forward bias voltages. Solid lines show the fit using Eqs. (2) and (3) .

observe a negative contribution to the capacitance below 10 KHz. This phenomenon is related to current relaxation that is due to electron-hole (e–h) recombination in the space charge limited current (SCLC) regime when the bipolar injection is predominant [30]. As shown in this figure, at sufficiently low frequencies and for V > 0.5 V, both capacitances curves converge to a constant negative value; while at sufficiently high frequencies the geometrical capacitance is obtained, $C_g = 2$ nF.

In admittance spectroscopy (AS), the material under investigation is sandwiched between an anode and a cathode. During the measurement, the sample admittance is measured under the superposition of an applied dc voltage V_{dc} and a small ac excitation v_{ac} at various frequencies. The frequency dependent admittance can be generally expressed [31] by:

$$Y(\omega) = \frac{1}{Z(\omega)} = \frac{i_{ac}}{v_{ac}} = G + i\omega C, \quad (2)$$

where i_{ac} is the ac current response, ω is the angular frequency, G and C are the conductance and the capacitance respectively.

According to many approaches which treated NC in organic semiconductor devices [30,32,33], the recombination time determined in the first section plays an important role to describe the NC in our device. Consequently, the effect of recombination on the capacitance can be summarized as follows [30]:

$$C(\omega) = \frac{-\chi\tau_r}{(1+\omega^2\tau_r{}^2)} \quad (3)$$

where $\chi$is a fitting parameter and τ_r is the recombination time determined in the first section. We have used the latter expression to fit the measured dynamic capacitance shown in Fig. 4.

Since the capacitance reflects the stored charge per applied voltages, the presence of space charge in the device (dielectric) gives rise to deviation from the geometrical capacitance. In the bipolar regime (bipolar current), the increase of stored space charge can be much larger as compared to a unipolar condition because of the compensation of positive and negative charge carriers [34,35]. Furthermore, under the conditions of bipolar injection, the active layer contains both electrons and holes. As a result, the rate of e-h recombination is finite as a consequence. There exists a finite volume in which electrons and holes overlap, resulting in recombination current which is proportional to the probability of recombination [36].

In Fig. 4, we show (Black solid lines) the fits to experimental data for the measured capacitance in the unipolar (0 V and 0.5 V) and bipolar (1 V and 1.5 V) injection regimes. The derived parameters for all bias voltages are summarized in Table 1.

From this table, we see that the recombination time τ_{rec}decreases with increasing bias voltages. This result is in agreement with the direct Langevin-type bimolecular recombination; when the bias voltage increases, the carrier density and mobility increase as a result τ_{rec}should decrease [32]. On the other hand, when the voltage increases, R_t and R_{rec} decrease. In fact, in the unipolar regime, this decrease is remarkable if compared to the bipolar regime in which both resistances are in the same order of magnitude. Our findings entail that the latter two resistances are affected by the voltage, this is in accordance with other works using P3HT and C_{60} combination [29]. Furthermore, from the fits to experimental data of Fig. 2, the C_μ increases with the increase of the applied forward bias voltages (see Table 1). This increase is expected as the density of states (DOS) occupancy progresses [23]. To reproduce theoretically the second semicircle shown in the cole–cole impedance plots shown in Fig. 2, we have taken R_{co} as negative values. The latter originality is due to the properties of metal/film interface. So, the origin of the negative values of R_{co} can be accounted for theoretically in terms of increasing coverage of the interface between AnE-PVstat: PCBM and LiF/Al when the applied forward bias voltages increase [37–39]. Moreover, the mobility of global carriers extracted from fits, both electrons and holes, exhibits a value approximately equal to 2 10^{-3} $cm^2V^{-1}s^{-1}$. This value is in good agreement with that derived using PCBM electron-only devices from J-V measurements, for which current is considered SCL, and, hence, electrical field driven rather than diffusion-determined [29].

4. Conclusion

To sum up, we have studied the impedance spectra (cole–cole plot) in an organic solar cell based on an ambipolar polymer AnE-PVstat. We found that in the bipolar regime, there are two arcs back toward the origin. To reproduce theoretically the cole–cole impedance plots, we have used an equivalent circuit which describes the realistic elements existing in the device. This equivalent circuit has been developed to provide insight into the physical mechanisms of frequency dependent charge transport and it suggests strategies for optimizing this behavior in many applications based on organic solar cell. Also, we have shown that NC at low frequencies occurs under bipolar injection and we have explained it by the e-h recombination. The time dependent recombination current leads to a negative contribution to the low frequency capacitance. We found that the recombination time decreases with the increase of the bias. This is consistent with a bimolecular recombination process.

Acknowledgements

D.A.M.E is grateful to the Deutsche Forschungsgemeinschaft for financial support in the framework of priority program SPP1355. D. A.M.E and N.S.S gratefully acknowledge the financial support from the Austrian Fund for Advancement of Science (FWF) within the Wittgenstein Prize scheme (Z222-N19 Solare Energieumwandlung). M. Radaoui thanks Mathiew White (Linz institute for Organic Solar Cells (LIOS) JKU University, Austria) for several helpful discussions.

References

[1] C.J. Brabec, N.S. Sariciftci, J.C. Hummelen, Adv. Funct. Mater. 11 (2001) 15–26.
[2] H. Hoppe, N.S. Sariciftci, J. Mater. Res. 19 (2004) 1924–1945.
[3] S. Gunes, H. Neugebauer, N.S. Sariciftci, Chem. Rev. 107 (2007) 1324–1338.
[4] C. Winder, N.S. Sariciftci, J. Mater. Chem. 14 (2004) 1077–1086.

[5] M. Kaltenbrunner, M.S. White, E.D. Głowacki, T. Sekitani, T. Someya, N.S. Sariciftci, S. Bauer, Nat. Commun. 3 (2012) 770.
[6] L. Dou, J. You, Z. Hong, Z. Xu, G. Li, R.A. Street, Y. Yang, Adv. Mater. 25 (2013) 6642–6671.
[7] M.A. Green, K. Emery, Y. Hishikawa, W. Warta, E.D. Dunlop, Prog. Photovoltaics: Res. Appl. 20 (2012) 12.
[8] I. Mora-Sero, J. Bisquert, F. Fabregat-Santiago, G. Garcia-Belmonte, G. Zoppi, K. Durose, Y. Proskuryakov, I. Oja, A. Belaidi, T. Dittrich, Nano Lett. 6 (2006) 640–650.
[9] V.G. Pedro, X. Xu, I. Mora-Sero, J. Bisquert, ACS Nano 4 (2010) 5783–5790.
[10] B.J. Leever, C.A. Bailey, T.J. Marks, M.C. Hersam, M.F. Durstock, Adv. Energy Mater. 2 (2012) 120–128.
[11] G. Garcia-Belmonte, P.P. Boix, J. Bisquert, M. Sessolo, H.J. Bolink, Sol. Energy Mater. Sol. Cells. 94 (2010) 366–375.
[12] G. Juska, K. Arlauskas, G. Sliaužys, A. Pivrikas, A.J. Mozer, N.S. Sariciftci, M. Scharber, R. Österbacka, Appl. Phys. Lett. 87 (2005) 222110.
[13] F.A. Castro, P.R. Bueno, C.F.O. Graeff, F. Noesch, L. Zuppiroli, L.F. Santos, R.M. Faria, Appl. Phys. Lett. 87 (2005) 013505.
[14] J. Bisquert, G. Garcia-Belmonte, A. Pitarch, H.J. Bolink, Chem. Phys. Lett. 422 (2006) 184–191.
[15] H.H.P. Gommans, M. Kemerink, G.G. Andersson, R.M.T. Pijper, Phys. Rev. B 69 (2004) 155216.
[16] A.G.U. Perera, W.Z. Shen, M. Ershov, H.C. Liu, M. Buchanan, W.J. Schaff, Appl. Phys. Lett. 74 (1999) 3167.
[17] M. Ershov, H.C. Liu, L. Li, M. Buchanan, Z.R. Wasilewski, A.K. Jonscher, IEEE Trans. Electron Devices 45 (1998) 2196–2206.
[18] L.S.C. Pingree, B.J. Scott, M.T. Russell, M.C. Hersam, Appl. Phys. Lett. 86 (2005) 073509.
[19] G.B. Parravicini, A. Stella, M.C. Ungureanu, R. Kofman, Appl. Phys. Lett. 85 (2004) 302.
[20] L. Bakueva, G. Konstantatos, S. Musikhin, H.E. Ruda, A. Shik, Appl. Phys. Lett. 85 (2004) 3567.
[21] G. Perrier, R. de Bettignies, S. Berson, N. Lemaitre, S. Guillerez, Sol. Energy Mater. Sol. Cells 101 (2012) 210–216.
[22] A. Mani, C. Huisman, A. Goossens, J. Schoonman, J. Phys. Chem. B 112 (2008) 10086–10091.
[23] G. García-Belmonte, A. Guerrero, J. Bisquert, J. Phys. Chem. Lett. 4 (2013) 877–886.
[24] D.A.M. Egbe, S. Türk, S. Rathgeber, F. Kühnlenz, R. Jadhav, A. Wild, E. Birckner, G. Adam, A. Pivrikas, V. Cimrova, G. Knör, N.S. Sariciftci, H. Hoppe, Macromolecules 43 (2010) 1261–1269.
[25] M. Radaoui, E. Hleli, Z. Ben Hamed, A. Ben Fredj, H. Hrichi, S. Romdhane, D.A.M. Egbe, H. Bouchriha, Mater. Sci. Semicond. Process. 30 (2015) 285–291.
[26] M.S. White, M. Kaltenbrunner, E.D. Głowacki, K. Gutnichenko, G. Kettlgruber, I. Graz, S. Aazou, C. Ulbricht, D.A.M. Egbe, M.C. Miron, Z. Major, M.C. Scharber, T. Sekitani, T. Someya, S. Bauer, N.S. Sariciftci, Nat. Photonics 7 (2013) 811–816.
[27] D.A.M. Egbe, B. Carbonnier, E. Birckner, U.W. Grummt, Prog. Polym. Sci. 34 (2009) 1023–1067.
[28] K.S.A. Butcher, T.L. Tansley, D. Alexiev, Solid State Electron. 39 (1996) 333–336.
[29] T. Ripolles-Sanchis, A. Guerrero, J. Bisquert, G. Garcia-Belmonte, J. Phys. Chem. C 116 (2012) 16925–16933.
[30] C. Lungenschmied, E. Ehrenfreund, N.S. Sariciftci, Organ Electron. 10 (2009) 115–118.
[31] K.K.H. Chan, S.W. Tsang, H.K.H. Lee, F. So, S.K. So, J. Pol. Sci. Part B: Pol Phys. 51 (2013) 649–658.
[32] N.A. Penin, Semiconductors 30 (1996) 340.
[33] A.G.U. Perera, W.Z. Shen, M. Ershov, H.C. Liu, M. Buchanan, W.J. Schaff, Appl. Phys. Lett. 74 (1999) 3167.
[34] H.H.P. Gommans, M. Kemerink, R.A.J. Janssen, Phys. Rev. B. 72 (2005) 235204.
[35] M.A. Lampert, P. Mark, Current Injection in Solids, 1st ed., Academic, London, 1970.
[36] M. Radaoui, M.A. Saidani, A. Ben Fredj, S. Romdhane, M. Havlicek, D.A.M. Egbe, N.S. Sariciftci, H. Bouchriha, J. Appl. Phys. 116 (2014) 183901.
[37] R.D. Armstrong, K. Edmondson, Electrochim. Acta 18 (1973) 937–943.
[38] M. Keddam, J.F. Lizee, C. Pallotta, H.J. Takenouti, J. Electrochem. Soc. 131 (1984) 2016–2024.
[39] E. Barsoukov, J. Ross Macdonald, Impedance Spectroscopy: Theory, Experiment, and Applications, 2nd ed., Wiley, New York, 2005, pp. 363–381.